Thermographic properties of Eu^{3+}- and Sm^{3+}-doped Lu_2O_3 nanophosphor

VESNA LOJPUR, ŽELJKA ANTIĆ, RADENKA KRSMANOVIĆ, MINA MEDIĆ, MARKO G. NIKOLIĆ and MIROSLAV D. DRAMIĆANIN*

Vinča Institute of Nuclear Sciences, University of Belgrade, P. O. Box 522, 11001 Belgrade, Serbia

Abstract: Samples of Lu_2O_3:Eu^{3+} (3 at. % Eu) and Lu_2O_3:Sm^{3+} (1 at. % Sm), were prepared *via* the polymer complex solution method using poly(ethylene glycol) as the fuel and as nucleation agent for crystallization process. Knowing that lutetium oxide has high chemical stability and temperature resistance, in this study, the possibility for its application in high-temperature phosphor thermometry was investigated. This non-contact technique uses the thermal dependence of phosphor fluorescence to measure temperature remotely. The structural and morphological properties were investigated by X-ray powder diffraction (XRPD) analysis and transmission electron microscopy (TEM). The obtained results confirmed that this synthesis yields the desired crystalline structure with particle sizes in the range from 30 to 50 nm. Photoluminescence emission measurements were recorded in the temperature range from ambient up to 873 K. The obtained results demonstrated the performance of Eu^{3+}- and Sm^{3+}-doped Lu_2O_3 as high temperature thermographic phosphors of very good sensitivity.

Keywords: Lu_2O_3; Eu^{3+}; Sm^{3+}; thermometry; FIR; luminescence.

INTRODUCTION

Rare-earth luminescent phosphor represents a very important group of materials since they find application in biomedical multicolor imaging, scintillators, high-energy physics, lamps and display devices, *etc.*[1–5] Recently, their application as temperature sensors has become very popular. In order to obtain an optical temperature sensor with appropriate characteristics, it is necessary to choose an adequate optically active ion and a suitable host matrix. Rare earth ions, such as Eu^{3+}, Sm^{3+}, Er^{3+}, Tm^{3+}, Ho^{3+} and Nd^{3+}, are luminescent activators that have coupled energy levels required for application in optical temperature sensors. These ions accommodate easily into a variety of different host materials. It is

1735

known that rare-earth sesquioxides are significant host materials due to their good chemical stability, thermal conductivity and high light output. Among them, lutetium oxide Lu_2O_3 represents a promising matrix material because of the high band gap between the valence and conduction bands ($\approx$5.8 eV), high melting point ($\approx$2763 K), very high mass density ($\approx$9.42 g cm^{-3}) and large atomic number ($Z = 71$) that contributes to a high stopping power for ionizing radiation. In addition, Lu_2O_3 has a cubic bixbyite crystalline structure with space group *Ia*-3 which is isostructural with the well-known Y_2O_3 structure.[6–8]

In order to avoid potential problems that could occur during synthesis in the solid phase, such as non-homogeneity, imprecise control of the cation stoichiometry and high processing temperature, it is more convenient to use wet chemical processes, such as hydrothermal synthesis, sol–gel, spray pyrolysis, co-precipitation, combustion synthesis, pulsed vapor deposition, *etc*.[9–15] In this study, the polymer complex solution (PCS) method, which is very simple, fast and cost-effective, was used. The PCS preparation procedure provides powders composed of well crystalline and uniform in size nanoparticles, which is a prerequisite for obtaining high-quality, transparent ceramics. The utility of the polymeric approach comes from the coordination of metal cations onto the poly(ethylene glycol) (PEG) chains during the gelation process, resulting in very low cation mobility. In this way, PCS provides mixing of constituting elements at the atomic level and allows homogeneous control of very small rare earth concentrations, providing in this way, a uniform structure of the materials.[16]

Thermographic phosphors (TPs) are oxides doped with rare earth or transition metal ions that emit visible, infrared or UV radiation upon excitation from an external energy source. Their luminescent properties, such as the positions and widths of the luminescence peaks, the intensities of the luminescence lines and decay lifetimes of luminescence, change with temperature. The fluorescence intensity ratio (FIR) method is based on the intensity ratio between two emission lines or areas in the PL spectrum. This technique is flexible and successful in measuring temperatures where conventional methods employing pyrometry, thermocouples or thermistors, may prove to be unsuitable. The intensity, wavelength or lifetime (duration of light) of the detected emission is used to determine the temperature of a surface. This approach is very precise, simple, non-intrusive with a wide temperature range (from 10 to 2000 K).[17,18]

Using this technique, very good results were previously obtained by measuring and comparing peak intensities and areas in different host matrixes.[19,20] Although, according to the literature, Lu_2O_3 proved itself to be a host material that gives better luminescent properties in comparison to Y_2O_3, it has not been sufficiently studied.[21] Hence, in the present study, Lu_2O_3 doped with either 3 at. % Eu^{3+} or 1 at. % Sm^{3+} prepared by combustion synthesis were elaborated as optical temperature sensors in the range from 293 to 823 K.

EXPERIMENTAL

Lutetium oxide doped with either 3 at. % Eu^{3+} or 1 at. % Sm^{3+} was fabricated by the polymer complex solution method. The starting materials, Lu_2O_3, Eu_2O_3 and Sm_2O_3 (all Alfa Aesar, 99.9 %), were appropriately measured and dissolved in hot nitric acid. To the obtained solutions, PEG (Alfa Aesar, $M_w = 200$) was added in a 1:1 mass ratio to the starting oxides, whereby metal–PEG solutions were formed. The solutions were continuously stirred at 80 °C for a few hours until solid complexes were formed that were subsequently combusted at 800 °C in air for 2 h, giving white powders as the resulting products.

The phase composition was investigated by X-ray powder diffraction analysis (XRPD) on a Philips PW 1050 instrument, using Ni filtered $CuK\alpha_{1,2}$ radiation. The diffraction data were recorded in the 2θ range from 10° to 120° counting for 12 s in each 0.02° step. The microstructure at the local level was analyzed by the TEM technique using a Philips/FEI CM300 electron microscope operating at 300 kV. The photoluminescence spectra were collected under the excitation light of a 450 W xenon lamp on a Fluorolog-3 model FL3-221 (Horiba Jobin-Yvon) spectroflurometer ($\lambda_{exc}(Lu_2O_3{:}Eu) = 393$ nm and $\lambda_{exc}(Lu_2O_3{:}Sm) = 406$ nm), elevating the temperature from ambient to 823 K in steps of 50 K.

RESULTS AND DISCUSSION

The X-ray diffraction pattern for the Lu_2O_3:3 at. % Eu sample is shown in Fig. 1. The XRD analysis confirmed that during calcination at 800 °C the sample crystallized in a cubic bixbyte crystal structure with the space group *Ia-3*. The peak positions were indexed according to the JCPDS card No. 12-0728 for the cubic Lu_2O_3 structure. The narrow peaks of high intensities imply good crystallinity of the sample.
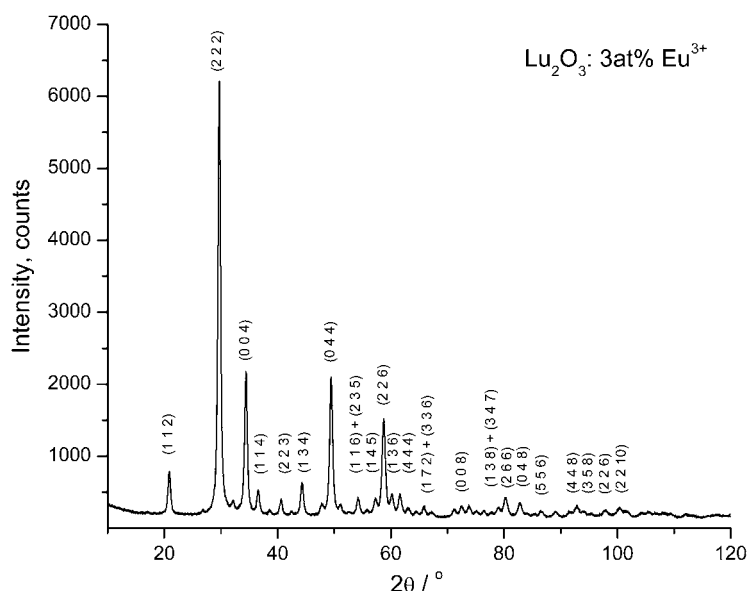

Fig. 1. XRD Pattern of Lu_2O_3:3 at. % Eu^{3+} nanopowder sample with diffraction peaks indexed according to JCPDS card No. 12-0728.

The morphology of Lu_2O_3:3 at. % Eu^{3+} sample analyzed with transmission electron microscopy (TEM) is presented in Fig. 2. The micrograph revealed the presence of agglomerates that consisted of nanoparticles in the range from 30 nm to 50 nm. High-resolution TEM (HR-TEM) showed a good crystalline structure without any irregularities, which are in good agreement with results obtained in the XRD measurements.
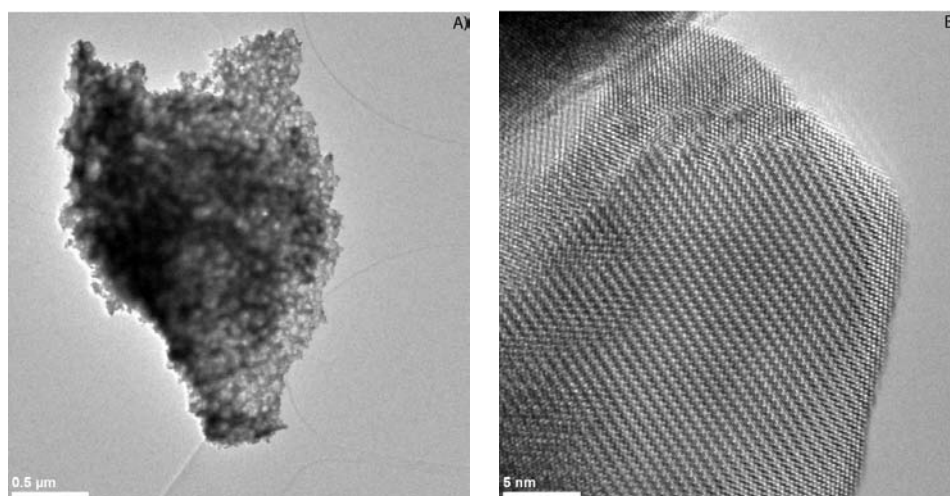

Fig. 2. Bright field image showing agglomerates of the powder sample with particle sizes ranging from 30–50 nm (A) and high-resolution images of constituting nanosized particles (B).

The FIR method is based on the selection of two emission lines from photoluminescent spectra and estimation of the temperature based on the ratio of their intensities. Two lines are considered appropriate for the intensity ratio method if they both have strong emission intensities over the whole temperature range and if their intensity ratio gives high temperature resolution.[22] This approach eliminates a number of errors arising from fluctuations of the excitation light source, temperature changes of excitation bands and non-uniform dopant concentrations. A special case of the FIR measurement technique involves using the fluorescence intensities from two closely spaced, "thermally coupled" energy levels, the relative population of which follows a Boltzmann type population distribution and is dependent on the temperature and the energy gap. Here, the ideal case was used, where the intensity of one of the emission lines is independent of temperature (internal reference); in this way, a calibration between the ratios of emissions is indicative of temperature. The main mechanism behind this phenomenon is thermalization: when two energy levels of the RE activator are closely separated by a difference of approx. 1000 cm^{-1}, the upper level will not emit fluorescence at low temperatures due to the high multi-phonon relaxation that quenches the energy.

With increasing temperature, the upper level becomes more populated and therefore the fluorescence from this level gradually increases at the expense of that of the lower level population.[23] The relative population between the two levels, R, which follows a Boltzmann-type population distribution, is given by:

$$R = \frac{I_{31}}{I_{21}} = C\exp(-\frac{\Delta E}{kT})$$ (1)

where k is the Boltzmann constant, $k = 0.695\,034\,76(63)$ cm⁻¹ K⁻¹, and $\Delta E = E_{32}$ is the energy gap between two excited levels (upper $i = 3$, lower $i = 2$, ground $i = 1$).

The rate at which the ratio R changes with temperature represents the sensor sensitivity, S:

$$S = \left|\frac{dR}{dT}\right| = R\left(\frac{\Delta E}{kT^2}\right)$$ (2)

For Eu³⁺, temperature could be determined using the FIR technique for the $^5D_1 \rightarrow {}^7F_1$ and $^5D_0 \rightarrow {}^7F_2$ transitions that have separation of approx. 1700 cm⁻¹ (Fig. 3a). At higher temperatures, the population of the $^5D_1$ level increases at the expense of the $^5D_0$ level population, causing an enhancement of emission intensity from the $^5D_1 \rightarrow {}^7F_1$ transition. The photoluminescence emission spectra of the (Lu₂O₃):3 at. % Eu³⁺ sample under excitation of 393 nm in the temperature range from 293–823 K are presented in Fig. 3b. Four characteristic emission bands from Eu³⁺ localized at around 580, 593, 611, 656 and 708 nm can be assigned to the $^5D_0 \rightarrow {}^7F_i$ ($i = 0, 1, 2, 3$ and 4) spin forbidden f–f transitions, respectively. The peak at 533 nm can be assigned to the $^5D_1 \rightarrow {}^7F_1$ transition. Obviously, at higher temperatures, the intensities of the emission band strongly decrease.

Dependence of emission intensities at 533, 580, 593 and 611 nm with temperature for Lu₂O₃:3 at. % Eu³⁺ sample are presented in Fig. 4. It is obvious that the peaks centered at 533, 580 and 593 nm are independent of temperature, while the peak centered at 611 nm gradually decreases with increasing temperature and exhibits a maximum value at 300 K.

The FIR relation was checked by recording the emission spectra at different temperatures from 293 to 823 K and the results are shown in Fig. 5. From the fit of these experimental data according to Eq. (1), the values $C = 3.06$ and $\Delta E = 1596$ cm⁻¹ were found, with a goodness of fit $R^2 = 0.9993$. The maximum sensor sensitivity calculated according to Eq. (2) is approximately 6×10^{-4} K⁻¹ at 823 K.

In the case of the Lu₂O₃:1 at. % Sm³⁺ sample, a schematic representation of the characteristic transitions is provided in Fig. 6a. Photoluminescence emission spectra of the sample under excitation of 406 nm in the temperature range from 293–823 K are presented in Fig. 6b. Three emissions at 578, 608 and 656 nm are
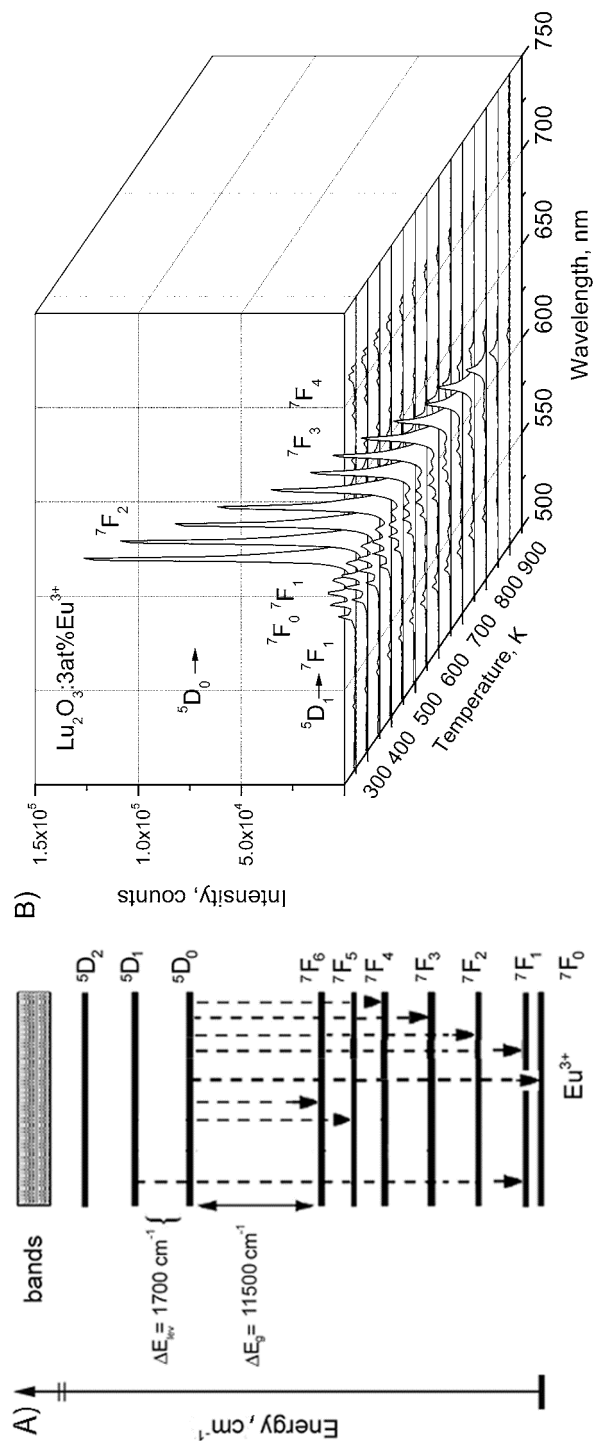
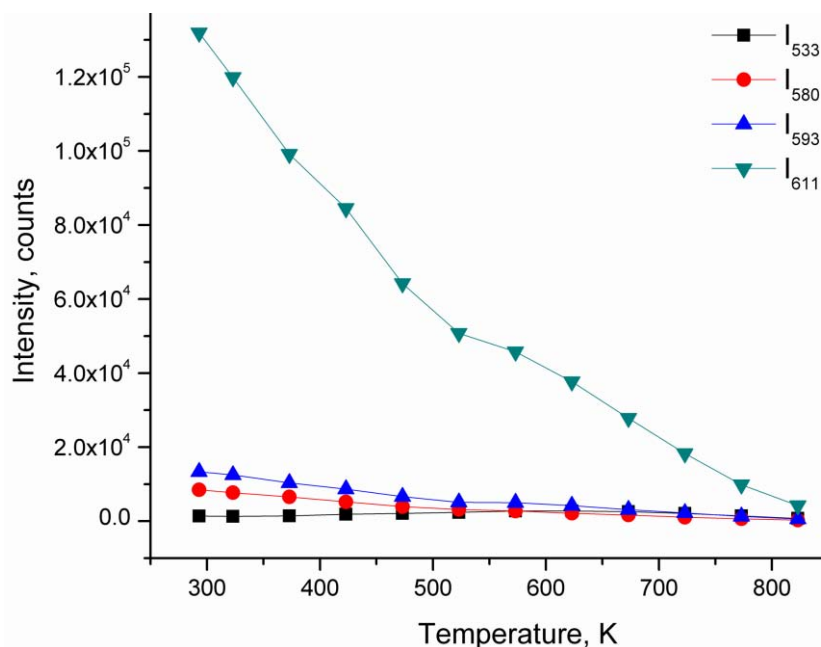Fig. 3. Energy level diagram for Eu^{3+} (A) and emission spectra at elevated temperatures (B).

Fig. 4. Temperature dependant variations of the selected peaks' intensity centered at 533, 580, 593 and 611 nm for Lu$_2$O$_3$:3 at. % Eu^{3+} sample. The sizes of the symbols represent the error of the measurements.

ascribed to the $^4G_{5/2} \rightarrow {}^6H_{5/2}$, $^6H_{7/2}$, $^6H_{9/2}$ transitions of Sm^{3+}, respectively. As internal reference, the $^4G_{5/2} \rightarrow {}^6H_{5/2}$ transition (emission line at 578 nm) was chosen.

The dependence of the emission intensities at 578, 608, and 656 nm on temperature for Lu$_2$O$_3$:1 at. % Sm^{3+} sample are presented in Fig. 7. In this case, the peaks centered at 608 and 656 nm gradually decreased with increasing temperature, while the peak centered at 578 nm showed irregular behavior with changing temperature.

The FIR of the emission at 578 nm relative to the emissions at 608 nm and 656 nm was checked by recording the emission spectra at different temperatures from 293 to 873 K and the results are presented in Fig. 8. From the fit of the obtained experimental data to Eq. (1), values of $C = 8.02$ and $\Delta E = 842.8$ cm^{-1} were found for $^4G_{5/2} \rightarrow {}^6H_{5/2}$, $^6H_{9/2}$, and $C = 4.16$, $\Delta E = 972.4$ cm^{-1} for the $^4G_{5/2} \rightarrow {}^6H_{5/2}$, $^6H_{7/2}$ transition ratio, with goodness of fits of 0.9871 and 0.9912, respectively. The maximum sensor sensitivities were approximately 3.6×10^{-3} K^{-1} at about 580 K for the $^4G_{5/2} \rightarrow {}^6H_{5/2}$, $^6H_{9/2}$ ratio and 1.6×10^{-3} K^{-1} at about 700 K for the $^4G_{5/2} \rightarrow {}^6H_{5/2}$, $^6H_{7/2}$ ratio.

A)

$$R = \frac{I_{533}}{I_{611}} = 3.06\exp{-\frac{2296.49}{T}}$$

B)

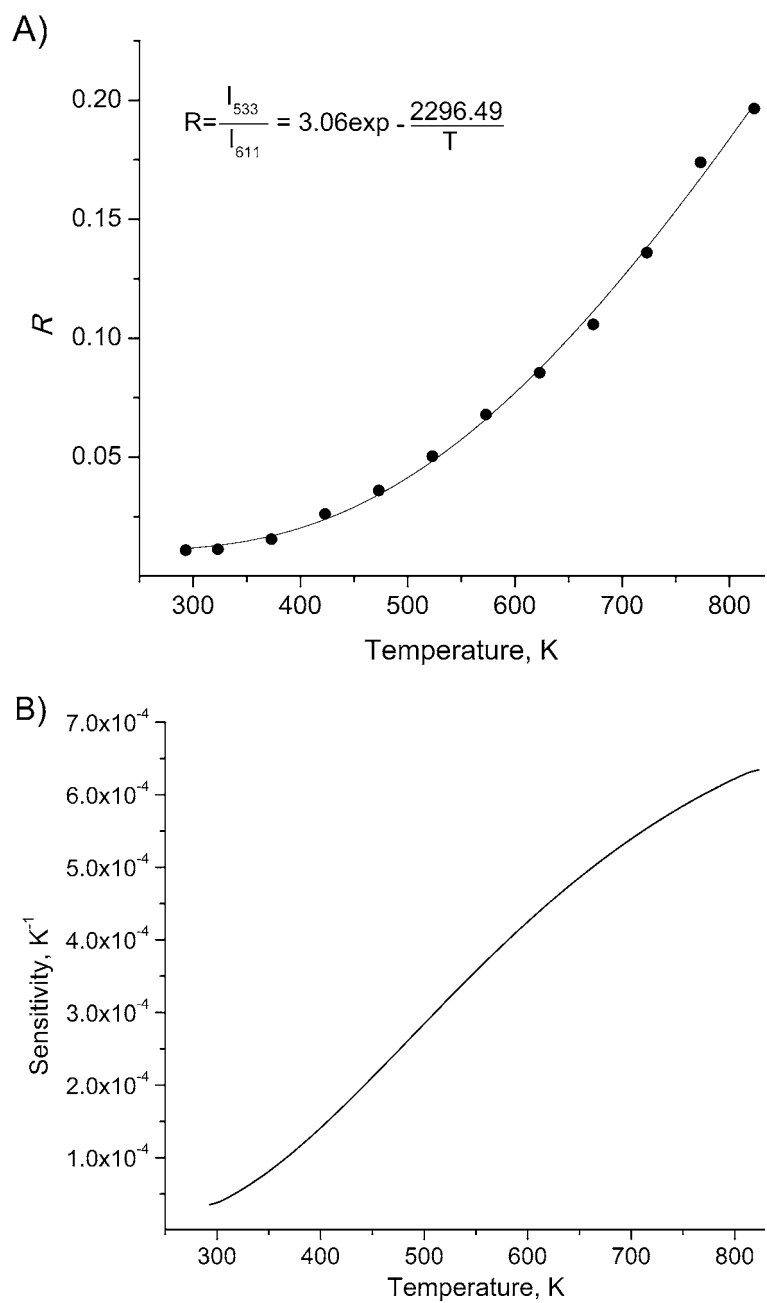Fig. 5. FIR of the $^5D_1 \rightarrow {}^7F_1$ and $^5D_0 \rightarrow {}^7F_2$ transitions for 3 at. % Eu^{3+} as a function of temperature.
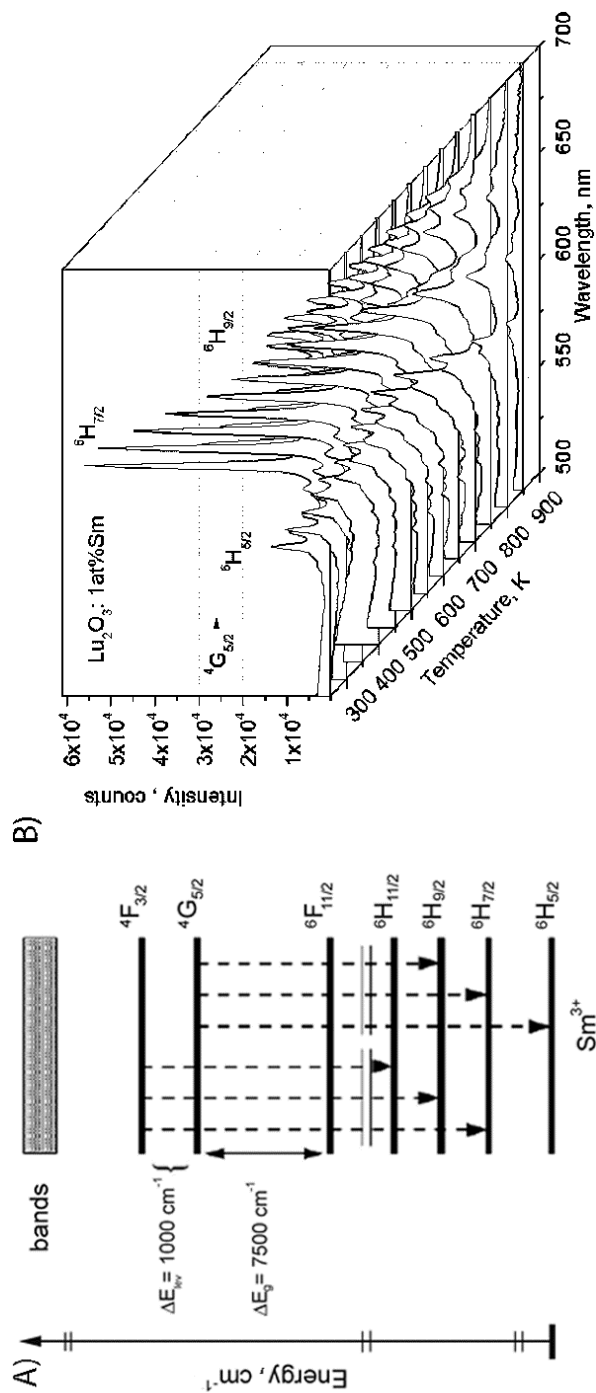
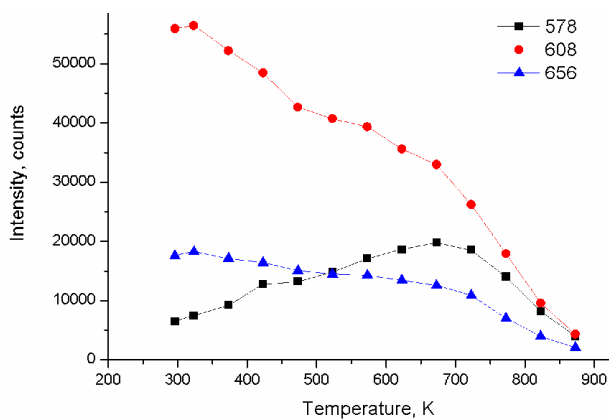Fig. 6. Energy level diagram for the Sm³⁺ (A) and emission spectra under elevated temperatures (B).

Fig. 7. Temperature dependant variations of the intensity of selected peaks centered at 578, 608 and 656 nm for the Lu_2O_3:1 at. % Sm^{3+} sample. The sizes of the symbols represent the error of the measurements.

A)

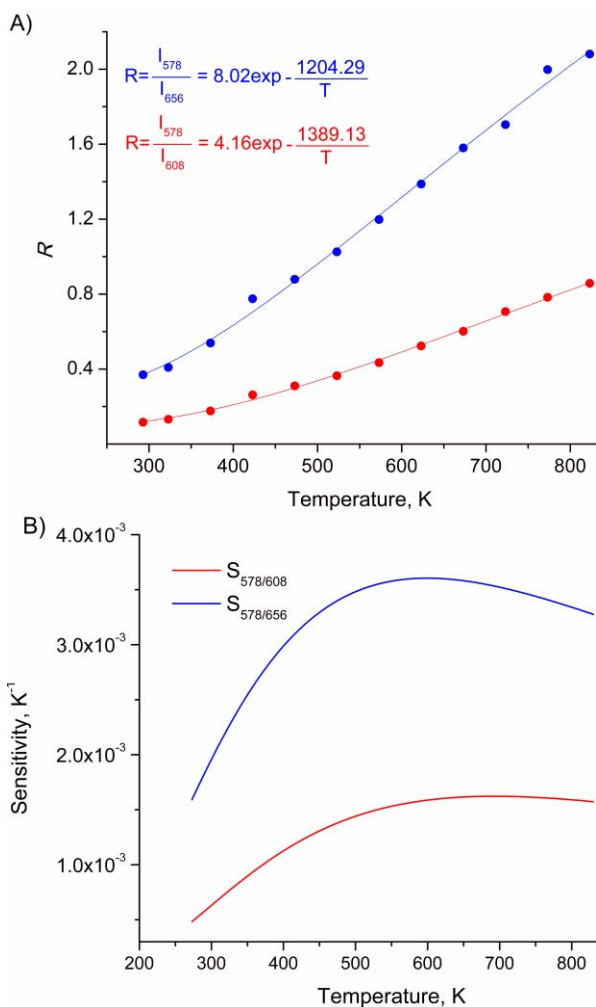$$R = \frac{I_{578}}{I_{656}} = 8.02\exp-\frac{1204.29}{T}$$

$$R = \frac{I_{578}}{I_{608}} = 4.16\exp-\frac{1389.13}{T}$$

B)

Fig. 8. FIR of the $^4G_{5/2} \rightarrow {}^6H_{5/2}$, $^6H_{9/2}$ and $^4G_{5/2} \rightarrow {}^6H_{5/2}$, $^6H_{7/2}$ transitions for 1 at. % Sm^{3+} as a function of temperature.

CONCLUSION

Lutetium oxide doped with either Eu^{3+} or Sm^{3+} was synthesized *via* the polymer complex solution method. The FIR technique was used to examine potential use of these materials in high-temperature phosphor thermometry. For Eu^{3+}, the emission intensity was monitored with increasing temperature for the main transitions $^5D_1 \rightarrow {}^7F_1$ and $^5D_0 \rightarrow {}^7F_2$, and detected the maximum sensitivity of approximately $6{\times}10^{-4}$ K^{-1} was detected at 823 K. For the Sm^{3+} ion, the $^4G_{5/2} \rightarrow \rightarrow {}^6H_{5/2}$, $^6H_{9/2}$ and $^4G_{5/2} \rightarrow {}^6H_{5/2}$, $^6H_{7/2}$ emission intensities were tracked and the maximum sensitivities of $3.6{\times}10^{-3}$ and $1.6{\times}10^{-3}$ K^{-1} were found at about 580 K and at about 700 K, respectively. Based on these results, it is evident that these materials could be used as temperature sensors at elevated temperatures.

И З В О Д

ТЕРМОГРАФСКА СВОЈСТВА Eu^{3+} И Sm^{3+} ДОПИРАНОГ Lu$_2$O$_3$ НАНОФОСФОРА

ВЕСНА ЛОЈПУР, ЖЕЉКА АНТИЋ, РАДЕНКА КРСМАНОВИЋ, МИНА МЕДИЋ, МАРКО Г. НИКОЛИЋ и МИРОСЛАВ Д. ДРАМИЋАНИН

Инсūиūуū за нуклеарне науке Винча, Универзиūеū у Беоīраду, ū. ūр. 522, 11001 Беоīрад

Узорци Lu$_2$O$_3$:Eu^{3+} (3 at. % Eu) и Lu$_2$O$_3$:Sm^{3+} (1 at. % Sm), су припремљени методом полимерног комплексног раствора уз коришћење полиетилен гликола као горива и нуклеационог агенса за процес кристализације. Узимајући у обзир да лутецијум-оксид има високу хемијску и температурску стабилност, у овом раду истражили смо могућност његове примене за високо-температурску термометрију. Ова термометријска метода је заснована на температурској зависност флуоресценце фосфора. Структурна и морфолошка својства су испитана коришћењем дифракције X зрака и трансмисионе електронске микроскопије. Добијени резултати су потвдили да примењена метода синтезе даје узорке жељене кристалне структуре, са честицама праха пречника од 30 до 50 nm. Фотолуминесцентна мерења су изведена у опсегу од собне температуре до 873 K. Остварени резултати показују да Eu^{3+} и Sm^{3+} допиран Lu$_2$O$_3$ има добре перформансе као високо-температурски термографски фосфор.

(Примљено 21. октобра, ревидирано 8. децембра 2012)

REFERENCES

1. E. Zych, M. Wawrzyniak, A. Kossek, J. Trojan-Piegza, L. Kepinski, *J. Alloy. Compd*. **451** (2008) 591
2. M. Xu, W. Zhang, N. Dong, Y. Jiang, Y. Tao, M. Yin, *J. Solid State Chem*. **178** (2005) 477
3. A. Garcia-Murillo, C. Le Luyer, C. Dujardin, T. Martin, C. Garapon, C. Pedrini, J. Mugnier, *Nucl. Ins. Methods, A* **486** (2002) 81
4. H. Wei, Z. Cleary, S. Park, K. Senevirathne, H. Eilers, *J. Alloy. Compd*. **500** (2010) 96
5. H. Guo, X. Yang, T. Xiao, W. Zhang, L. Lou, J. Mugnier, *Appl. Surf. Sci*. **230** (2004) 215
6. A. Martinez, J. Morales, L. A. Diaz-Torres, P. Salas, E. De la Rosa, J. Oliva, H. Desirena, *Mater. Sci. Eng., B* **174** (2010) 164

7. A. N. Gruzintsev, G. A. Emelchenko, Yu. V. Yermolayeva, V. M. Masalov, A. V. Tolmachev, P. Benalloul, C. Barthou, *Phys. Solid State* **53** (2011) 1263
8. L. An, J. Zhang, M. Liu, S. Chen, S. Wang, *Opt. Mater.* **30** (2008) 957
9. M. Kottaisamy, D. Jeyakumar, R. Jagannathan, M. M. Rao, *Mater. Res. Bull.* **31** (1996) 1013
10. P. D. Volanti, V. I. Rosa, C. E. Paris, A. C. Paskocimas, S. P. Pizani, *Opt. Mat.* **31** (2009) 995
11. C. Dujardin, C. Le Luyer, C. Martinet, C. Garapon, J. Mugnier, A. G. Murillo, C. Pedrini, T. Martin, *Nucl. Ins. Methods, A* **537** (2005) 237
12. M. Nichkova, D. Dosev, S. J. Gee, B. D. Hammock, I. M. Kennedy, *Anal. Chem.* **77** (2005) 6864
13. W. Q. Chen, Y. Shi, Q. L. An, W. S. Wang, J. Y. Chen, L. J. Shi, *J. Eur. Ceram. Soc.* **27** (2007) 191
14. S. Cho, H. Lee, C. Moon, J. Kim, J. Park, G. Jeon, R. Lee,, S. Nam, *J. Sol–Gel Sci. Technol.* **53** (2010) 171
15. C. Martinet, A. Pillonnet, J. Lancok, C. Garapon, *J. Lumin.* **126** (2010) 807
16. R. Krsmanovic, Z. Antic, B. Bartova, M. D. Dramicanin, *J. Alloy. Compd.* **505** (2010) 224
17. S. A. Wade, S. F. Collins, G. W. Baxter, *J. Appl. Phys.* **94** (2003) 4743
18. S. K. Singh, K. Kumar, B. S. Rai, *Sensor Actuat., A* **149** (2009) 16
19. M. G. Nikolic, D. J. Jovanovic, V. Đordjevic, Z. Antic, R. M. Krsmanovic, M. D. Dramicanin, *Phys. Scr.* **T149** (2012) 014063
20. V. Lojpur, M. Nikolic, L. Mancic, O. Milosevic, M. D. Dramicanin, *Ceram. Int.* **39** (2013) 1129
21. F. Vetrone, J. C. Boyer, J. A. Capobianco, A. Speghini, M. Bettinelli, *J. Phys. Chem., B* **106** (2002) 5622
22. J. Petit, B. Viana, P. Goldner, J. P. Roger, D. Fournier, *J. Appl. Phys.* **108** (2010) 123108
23. L. Liu, Y. Wang, X. Zhang, K. Yang, Y. Bai, C. Huang, Y. Song, *Opt. Commun.* **284** (2011) 1876.